Journal of Magnetism and Magnetic Materials 473 (2019) 205–214

Contents lists available at ScienceDirect

Journal of Magnetism and Magnetic Materials

journal homepage: www.elsevier.com/locate/jmmm

Research articles

Physical characterization and uptake of iron oxide nanoparticles of different prostate cancer cells

Maryam Youhannayee[a], Saeideh Nakhaei-Rad[b], Fereshteh Haghighi[b], Karsten Klauke[c], Christoph Janiak[c], Mohammad Reza Ahmadian[b], Robert Rabenalt[d], Peter Albers[d], Mathias Getzlaff[a,*]

[a] Institut für Angewandte Physik, Heinrich-Heine Universität, Düsseldorf, Germany
[b] Institut für Biochemie und Molekularbiologie II, Medizinische Fakultt der Heinrich-Heine Universität Düsseldorf, Germany
[c] Institut für Bioanorganische Chemie, HHU, Düsseldorf, Germany
[d] Klinik für Urologie, Universitätsklinikum Düsseldorf, Germany

ARTICLE INFO

Keywords:
Hyperthermia
Magnetite nanoparticles
Aminosilane
PC3 and BPH1 cell line

ABSTRACT

Among nanoparticles, magnetic nanoparticles are the most appealing candidate for diagnosis and cancer therapy. The researchers are tempting to improve the particles properties, including the size, shape, coating, and magnetic behavior or heating characteristics. Core shell type of magnetic nanoparticle is an important property that modulates their internalization *via* normal and cancer cells. In this study, magnetite nanoparticles (MNP) covered by N-(2-aminoethyl)-3-aminopropyltriethoxysilane (aminosilane – APTES) were synthesized by co-precipitation of aqueous solution of ferric chloride and ferrous sulfate iron salts with ammonium hydroxide as a base and functionalized by APTES to increase the viability and affinity of the particles to the cancer cells. The structural and morphological properties of these particles were characterized by transmission electron microscopy (TEM), X-ray diffraction (XRD) and Fourier transformed infrared spectroscopy (FTIR). 3-(4,5-dimethyl-2-thiazolyl)-2,5-diphenyl tetrazolium bromide (MTT assay) was carried out, to check the viability of the cells treatment with MNP and APTES-MNP. To study the cellular uptake *in vitro*, two prostate cell lines were investigated: PC3 as a cancerous cell line and BPH1 as a benign epithelial cell line (normal cells). Both cell lines were incubated for 24 h with different concentrations of MNP and APTES-MNP (100 and 500 µg/ml and one untreated sample as control). TEM and flow cytometry (FC) analyses were subsequently carried out to monitor the cellular uptake of MNP and APTES-MNP. FC data revealed an increase in cell granularity following the treatment with high concentration of the particles. Data showed that PC3 cancer cells take up more APTES-MNP with respect to control cells than BPH1 benign cells and in contrast BPH1 cell uptake MNP correlated to control cells more efficient than PC3 cells. The results from FC and TEM analyses demonstrate increasing of affinity of particles to cancer cell line (PC3). In this project we investigated the effect of surface functionalization of NP to affinity of the MNP and APTES-MNP on PC3 cells as a malignancy prostate cell and BPH1 benign cells as a normal cells. This approach may help to optimize the efficiency of hyperthermia for prostate cancer through internalization of particles to the cells or attaching to the membrane.

1. Introduction

In recent years, iron oxide nanoparticles and especially magnetite (Fe_3O_4) nanoparticles are considered as useful materials for biological and biomedical applications like magnetic resonance imaging, drug delivery, cell separation and hyperthermia due to, e.g., their biocompatibility and low toxicity [1–4]. To improve the magnetite nanoparticles' applications, their internalization to the target cells play a critical role. One criterion is the affinity of particles to the cell membrane. Therefore, different types of surface coating have been taken [5–11] to investigate the uptake of the particles into specific target cells.

APTES is a very prevalent coupling agent and forms a monolayer of aminosilane on the MNP surface by changing the surface decoration [12–16]. This tiny monolayer film with (-NH_2) active groups is a platform for additional bio-functionalization and increases the

* Corresponding author at: Institut für Angewandte Physik, Heinrich-Heine Universität, Universitätstr. 1, Gebäude 25.43, 40255 Düsseldorf, Germany.
E-mail address: Mathias.getzlaff@uni-duesseldorf.de (M. Getzlaff).

https://doi.org/10.1016/j.jmmm.2018.10.062
Received 22 June 2018; Received in revised form 21 September 2018; Accepted 13 October 2018
Available online 15 October 2018
0304-8853/

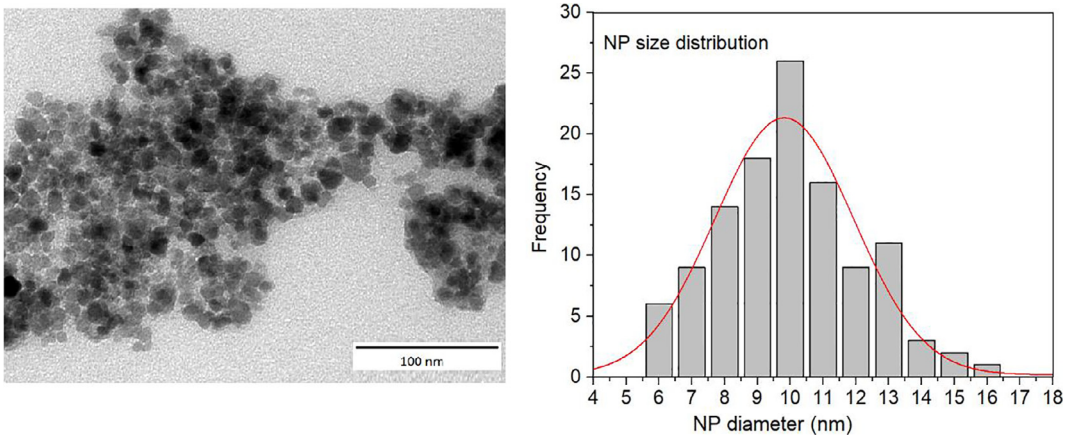

Fig. 1. (a) TEM images for aminosilane coated magnetite nanoparticles (APTES-MNP). (b) Related size distribution histogram of coated magnetite nanoparticles.

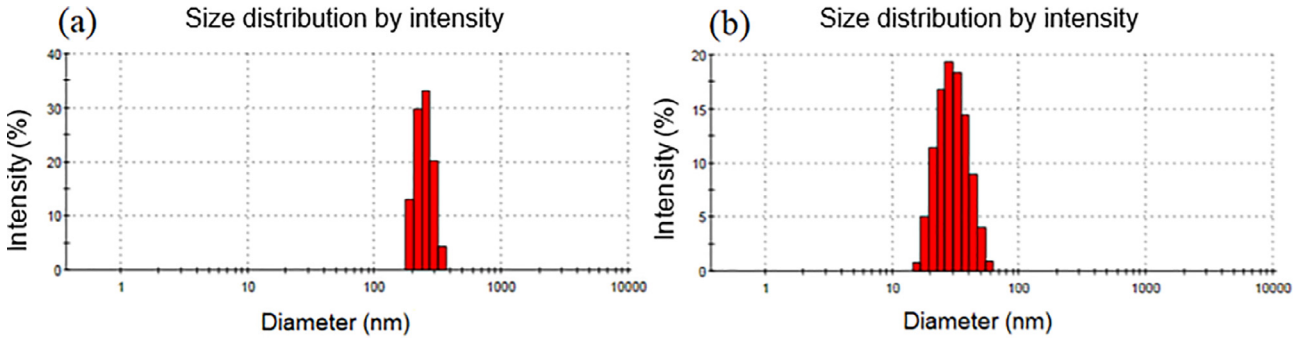

Fig. 2. DLS histogram of (a) MNP and (b) APTES-MNP. The significant smaller hydrodynamic diameter of the coated particles is observed due to the stability and decreased aggregation of the particles after coating.

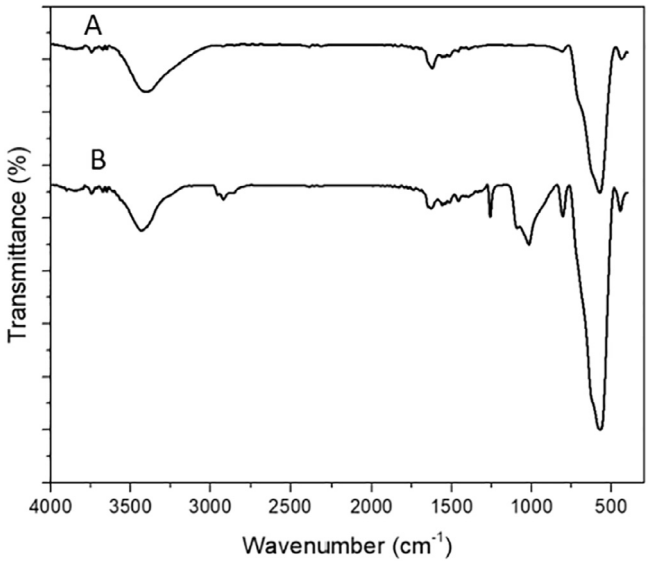

Fig. 3. FTIR spectra of (A) uncoated and (B) coated magnetite nanoparticles.

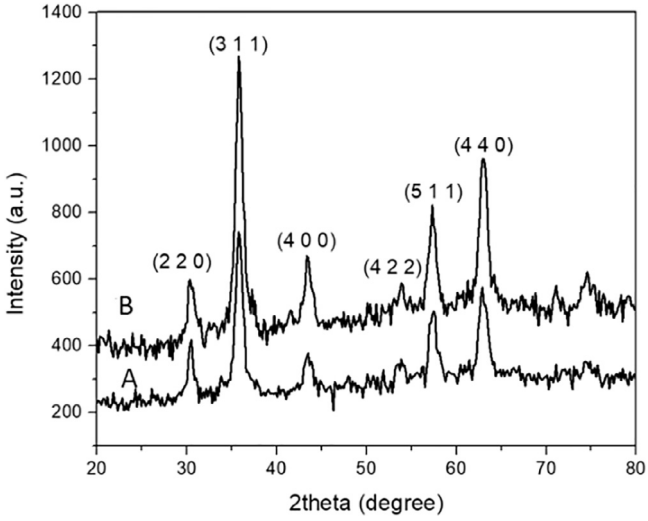

Fig. 4. XRD of (A) uncoated and (B) coated magnetite nanoparticles.

internalization of MNP to the cells. Due to the aminosilane shell, the uptake of the nanoparticles occurs due to endocytosis [17,18].

In this study, we synthesized the magnetite nanoparticles with aminosilane coating and characterized the particles' properties. Subsequently, we investigated the internalization of coated and uncoated nanoparticles after treatment of prostate cancer cells (PC3 cell line) and prostate benign cells (BPH1 cell line) by application of TEM and flow cytometry.

2. Materials and methods

2.1. Reagents and material

Ferric chloride ($FeCl_3 \bullet 6H_2O$, 99\%, CAS NO.10025-77-1) was purchased from ROTH company and ferrous sulfate ($FeSO_4 \bullet 7H_2O$, 99,5\%-CAS NO.7782-63-0) from ACROS company (USA). Ammonium hydroxide (NH_4OH, 25\%, CAS NO.1336-21-6) was obtained from VWR company. 3-Aminopropyltriethoxysilane ($NH_2(CH_2)_3Si\ (OC_2H_5)_3$, APTES) was purchased from SIGMA ALDRICH,

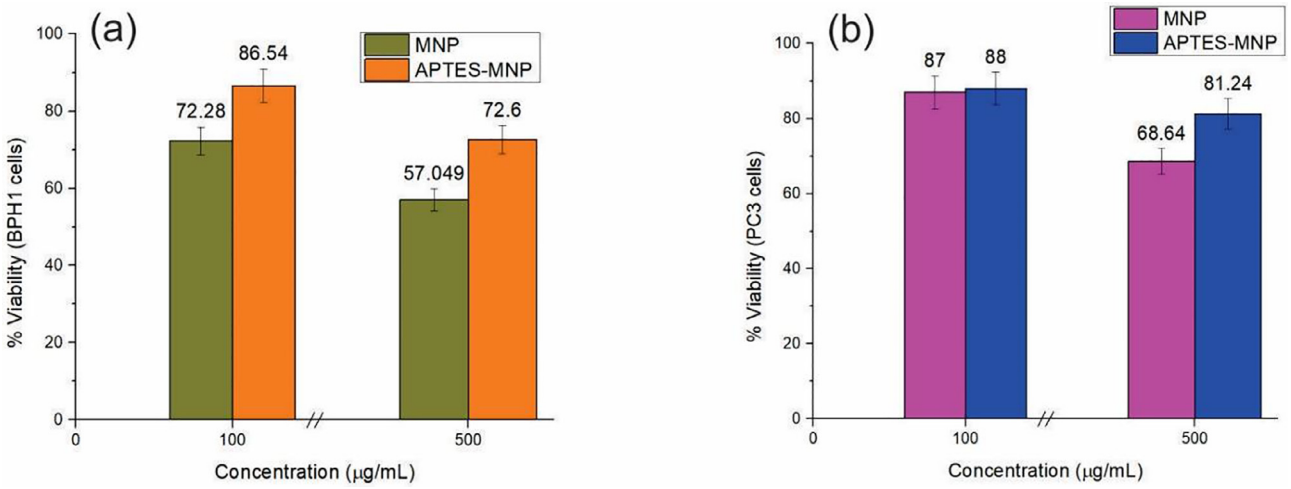

Fig. 5. MTT analysis of cell viability of BPH1 cells (a) and PC3 cells (b) shows the decreased the cell viability depending on concentration of coated and uncoated MNPs.

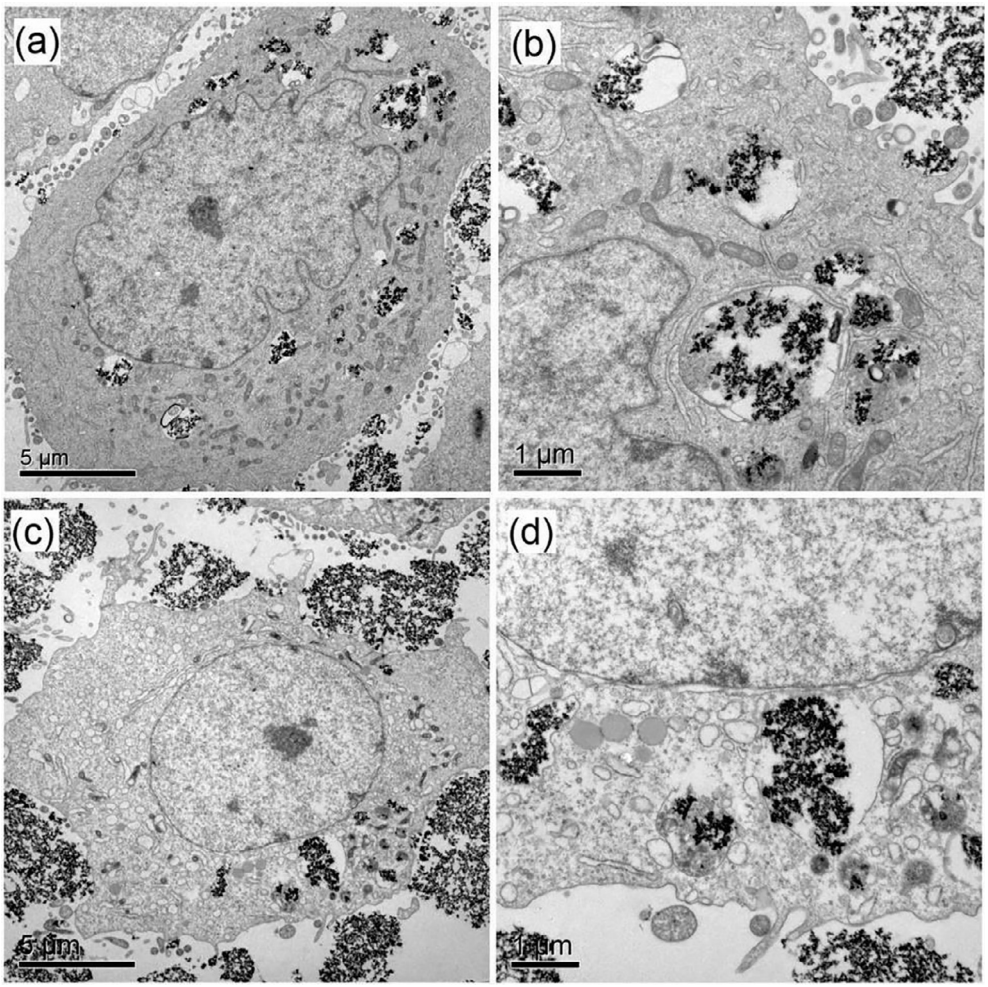

Fig. 6. TEM images of PC3 cells fixed after treatment and incubation for 24 h with uncoated nanoparticles (MNP): treatment with 100 μg/ml (a, b) and 500 μg/ml (c, d) with magnification of 5000× (a, c) and 15000× (b, d).

Germany. The PC3 prostate cancer cell line was from Professor Schulz group (Research Institute of Urology) and the BPH1 benign cell line from Professor Ahmadian group (Institute of Biochemistry and Molecular Biology, Heinrich Heine Universität, Düsseldorf).

2.2. Synthesis of magnetite nanoparticles (MNP)

Magnetite nanoparticles were synthesized as described previously by Molday [19], *via* the standard co-precipitation method, magnetic nanoparticles precipitated by adding alkali solution to Fe (II) and Fe

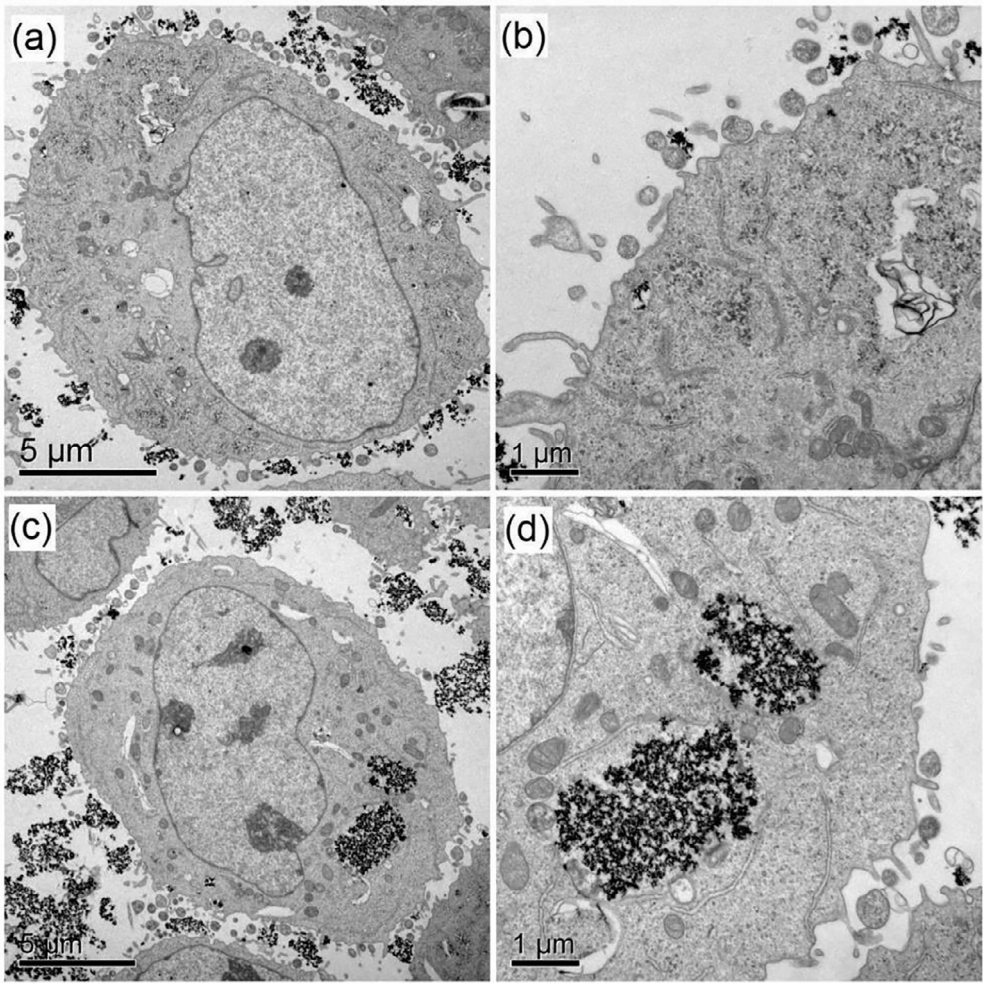

Fig. 7. TEM images of BPH1 cells fixed after treatment and incubation for 24 h with uncoated nanoparticles (MNP): treatment with 100 µg/ml (a, b) and 500 µg/ml (c, d) with magnification of 5000× (a, c) and 15000× (b, d).

(III) solution (molar ratio 2:1). Briefly, $FeCl_3 \cdot 6H_2O$ (2.704 g, 0.0196 mol) and $FeSO_4 \cdot 7H_2O$ (1.3704 g, 0.0095 mol) was dissolved in 180 ml distilled water while N_2 gas was flowing through a three-necked flask under vigorous mechanical stirring. After sufficiently stirring of the iron salt, 5.5 ml of ammonium hydroxide (NH_4OH) was injected abruptly in one portion to the reaction mixture by a 10 ml syringe while continuing stirring with the same speed (1000 rpm) for an additional half an hour. Due to addition of the alkaline solution the color of the mixture changed from orange to brown and finally black which shows the formation of MNPs precipitation immediately. In order to decrease the pH from 9.5 to 7 and to remove the residual ions the black solution was washed by magnetic separation with distilled water and ethanol. At the end, magnetite nanoparticles were dispersed in ethanol for the subsequent coating procedure.

2.3. Coating procedure

70 mg of obtained magnetite nanoparticles in solution was dissolved in 150 ml of ethanol and 1 ml of water and sonicated for 5 min [20]. After sonication, 35 µl of 3-aminopropyltriethoxysilane ($NH_2(CH_2)_3Si(OC_2H_5)_3$, APTES) was added to the reaction environment while mechanically stirring (1000 rpm) for 7 h. The aminosilane coated particles were obtained after washing 5 times with ethanol.

2.4. Characterization

In order to determine the particles' size, distribution and morphology, transmission electron microscopy measurements were carried out. In this experiment a TEM Zeiss 902, 80 kV was used. To prepare the TEM sample, one drop of the diluted sample deposited on a copper grid (Formvar/carbon film on 200 mesh nets, Plano Company, Germany) was dried for approximately one hour. An X-ray powder diffraction system (XRD, BRUKER D2 Phaser) with Cu-Kα_1 = 1.54056 Å was used to characterize the crystalline structure of MNP with and without coating in the 2θ range from 10 to 80 degrees. Dynamic light scattering (DLS) (Zetasizer Nano from Malvern Company) was used to measure the hydrodynamic diameter D_H of the nanoparticles by dilution of a few drops of the prepared nanoparticles in distilled water and also one filtered probe (with 0.2 µm filter) for each sample.

The Fourier transformed infrared (FTIR) measurements were carried out with a Bruker Tensor 37 in MIR (Mid Infrared) range (400–4000 cm^{-1}) through a KBr disc at room temperature to characterize the bands due to vibration of different functional groups for the uncoated and coated MNP.

2.5. Cell experiments

2.5.1. Cell culture

PC3 (prostate cancer epithelial cell) and BPH1 (benign prostate hyperplastic epithelia cell) were cultured in RPIM 1640 medium (ThermoFisher, 11875093) supplemented with 10% fetal bovine serum (FBS) (ThermoFisher, 10270-106) and 5% penicillin–streptomycin (Genaxxon bioscience, M3140.0100).

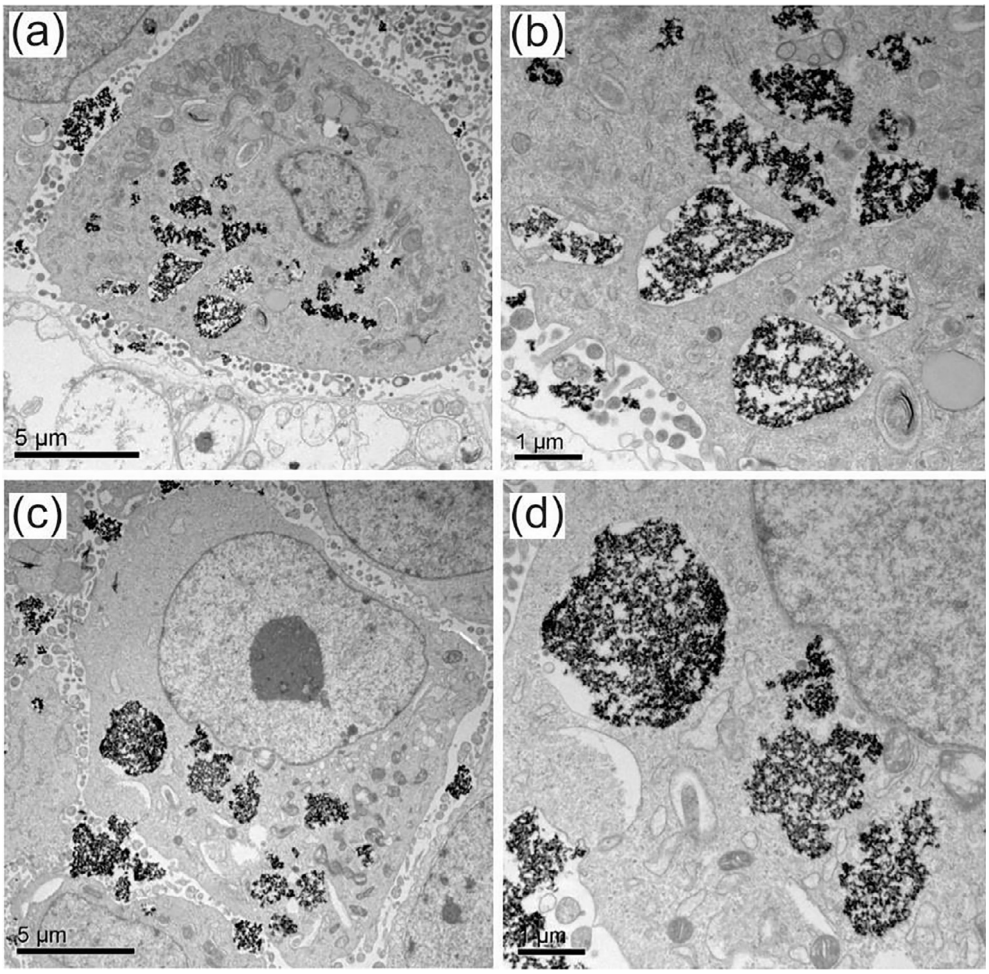

Fig. 8. TEM images of PC3 cells fixed after treatment and incubation for 24 h with APTES-MNP: treatment with 100 µg/ml (a, b) and 500 µg/ml (c, d) with magnification of 5000× (a, c) and 15000× (b, d).

2.5.2. Cell viability

3-(4,5-Dimethyl-2-thiazolyl)-2,5-diphenyl tetrazolium bromide (MTT assay) was used to evaluate the cell viability after treatment by the nanoparticles according to Mosmann [21]. 5 mg/ml of tetrazolium salt were dissolved in PBS and filtered to sterilize. When the PC3 and BPH1 cells reached the confluency of 70–80%, they were treated with 100 and 500 µg/ml of MNP and APTES-MNP in a 96-well plate in 37 °C. After 24 h, the cells were washed three times to remove the rest of the particles. The MTT was added and incubated with 10% (20 µl per 200 µl medium) concentration for 4 h to form formazan crystals and then 150 µl DMSO was added per well to dissolve the formazan crystal. The quantity of formazan is proportional to the viable cells. An ELIZA reader was used to record the absorbance changes at 570 nm.

2.5.3. Transmission electron microscopy

To investigate the internalization of the particles to the cells, a TEM (Hitachi H600, 75 kV) was used. For embedding the cells, they were fixed with 2,5% glutaraldehyde, 4% paraformaldehyde in 0,1 M cacodylate buffer solution for at least 2 h. Subsequently, the cells were washed and fixed with cacodylate buffer and osmium tetroxide (2%) respectively, dehydrated with 70–100% acetone and embedded in spur and cut in a tiny film using an ultra-microtome.

2.5.4. Flow cytometry

PC3 and BPH1 cells were treated with 100 and 500 µg/ml of MNP and APTES-MNP for 24 h. For flow cytometric analysis, single-cell suspensions were obtained with trypsin and the cells were washed with ice-cold PBS. The cells were fixed in 4% paraformaldehyde (PFA; Merck) for 10 min on ice, followed by two times washing with PBS. The samples were analyzed with FACS Canto II (BD Pharmingen). Evaluation of data was carried out with “Flowing software” (version: 2. 5. 1) (Turku Center for Biotechnology, University of Turku, Finland).

3. Results and discussion

After the synthesis of APTES-MNP and a subsequent treatment of the cells by particles, different characterization techniques were carried out: TEM measurement to determine the particles’ size, XRD to characterize the crystalline structure of the nanoparticles and FTIR to acquire knowledge of the chemical components of the ligand shell. For the cells treatments, TEM and flow cytometry were carried out to investigate the internalization of particles to cells.

3.1. Characterization of APTES-MNP nanoparticles

Fig. 1a shows the TEM image of quasi-spherical magnetite nanoparticles coated with APTES. The average diameter of the metallic core is about 10 nm (s. Fig. 1b) which can be seen from the distribution of the particle diameter according to TEM measurements. The size of the nanoparticles was measured by calculating the ratio of the particle to the figure scale bar in pixel with help of a graphic software and the Origin pro version 9 program.

The hydrodynamic size of nanoparticles is measured by DLS. The DLS data of MNP and APTES-MNP are presented in Fig. 2a and b,

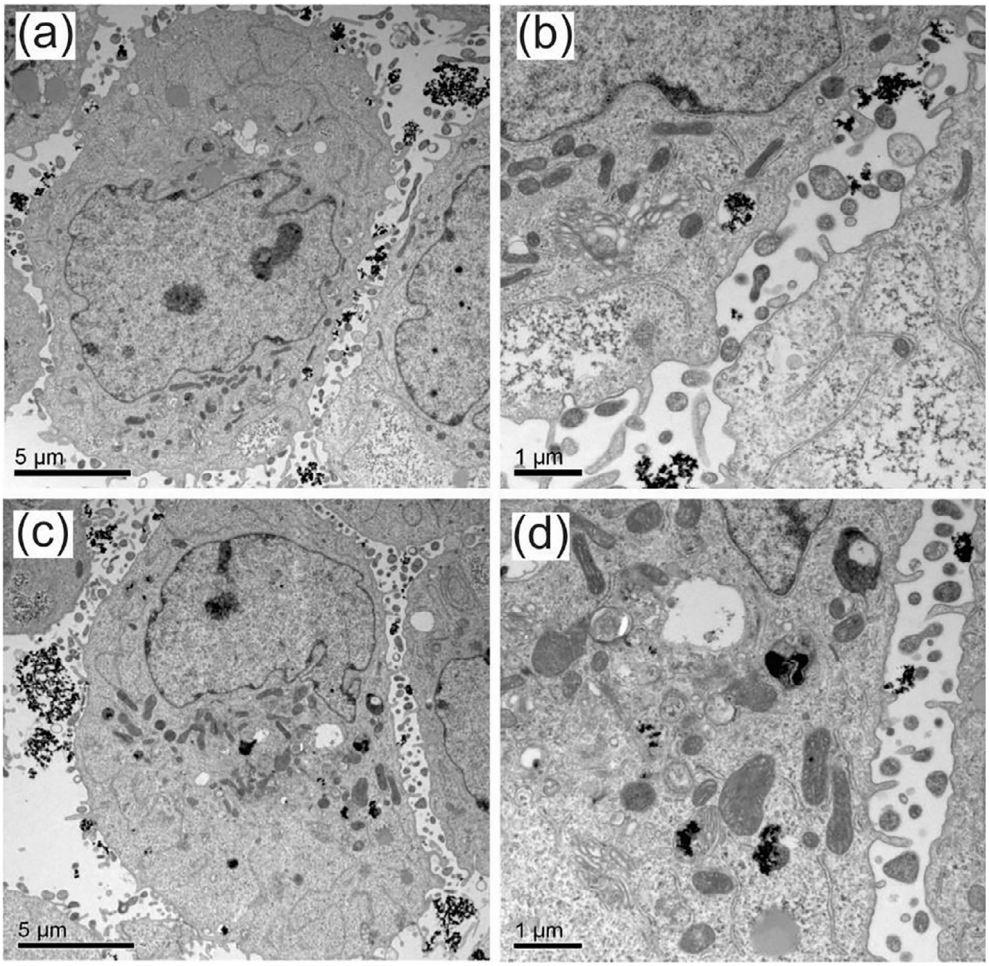

Fig. 9. TEM images of BPH1 cells fixed after treatment and incubation for 24 h with APTES-MNP: treatment with 100 µg/ml (a, b) and 500 µg/ml (c, d) with magnification of 5000× (a, c) and 15000× (b, d).

respectively. The larger size of the particles are measured in comparison by TEM which can be cause by forming of particles agglomeration due to magnetic interaction of nanoparticles [22]. DLS analysis illustrated larger particles for MNP than APTES-MNP which can be interpreted such that the coating of the particles increased the stability that resulted in less agglomeration for APTES-MNP.

The stable coating with the APTES molecules is due to the large surface-to-volume ratio of the nanoparticles, the high surface activity, and the OH-rich surface [23]. This is shown in Fig. 3 by comparing the FTIR spectra of magnetite nanoparticles without coating (A) and with coating (B). Fe-O bonds in bulk magnetite has ν_1 and ν_2 band at 570 cm^{-1} and 375 cm^{-1}, respectively [24]. The FTIR spectra in Fig. 3 show two absorption bands at around 568 cm^{-1} and 621 cm^{-1} which result from splitting of the ν_1 band. The band at 441 cm^{-1} comes from a shift of the ν_2 band. In comparison to the coated magnetite nanoparticles, FTIR spectra of APTES–MNP show additional absorption bands at 2855 cm^{-1} and 2920 cm^{-1} due to stretching vibrations of C–H bonds. The bands at 1017 cm^{-1} and 1091 cm^{-1} result from stretching vibrations of Si–O. The band at 804 cm^{-1} is due to $–NH_2$ vibration which only occur for aminosilane coated magnetite nanoparticles. To determine the crystalline structure of the magnetite nanoparticles with and without functionalization, XRD measurements have been carried out. The XRD pattern confirm the cubic inverse structure of both MNP and APTES-MNP with their characteristic peaks (2 2 0), (3 1 1), (4 0 0), (4 2 2), (5 1 1) and (4 4 0) being shown in XRD pattern in Fig. 4 which is in a good agreement with literature [25]. The XRD results prove that magnetite nanoparticles coated with APTES do not change the crystalline structure.

3.2. Cell viability (MTT)

The BPH1 and PC3 cells were treated for 24 h with 100 and 500 µg/mL of MNP and APTES-MNP and the cell viability was measured by MTT assay Fig. 5. In both cell line, the higher viability is observed for coated nanoparticles (APTES-MNP). The BPH1 cells treated with 100 µg/ml MNP, shows 72% (MNP) and 86% (APTES-MNP) viability and lower levels of toxicity was observed for PC3 cells 83% and 85%. This trend is also seen in concentration of 500 µg/ml. The higher concentration of the MNP results in the lower cell viability for both tested cell lines. Collectively, in both conditions PC3 cells illustrated more viability than BPH1 cells. In the same line of evidence, Naqvi and colleagues reported after 6 h of treatment with MNP 95% viability at the concentration 25–200 µg/ml and 55%-65% viability at the higher concentration 300–500 µg/ml [26].

3.3. In vitro investigation of particle internalization by the cells

In order to compare the effect of surface functionalization in NP uptaking and the mechanism of the internalization, the cellular uptake of MNP and APTES-MNP with different concentrations of 100 and 500 µg/ml, was examined for two cell lines of PC3 and BPH1 by TEM (s. Figs. 6–9) and flow cytometry (s. Figs. 10, 11, 12, and 13). The cells were seeded on 6-well plates and after reaching 70% to 80% confluency, were treated with MNP for 24 h. We observed that after the

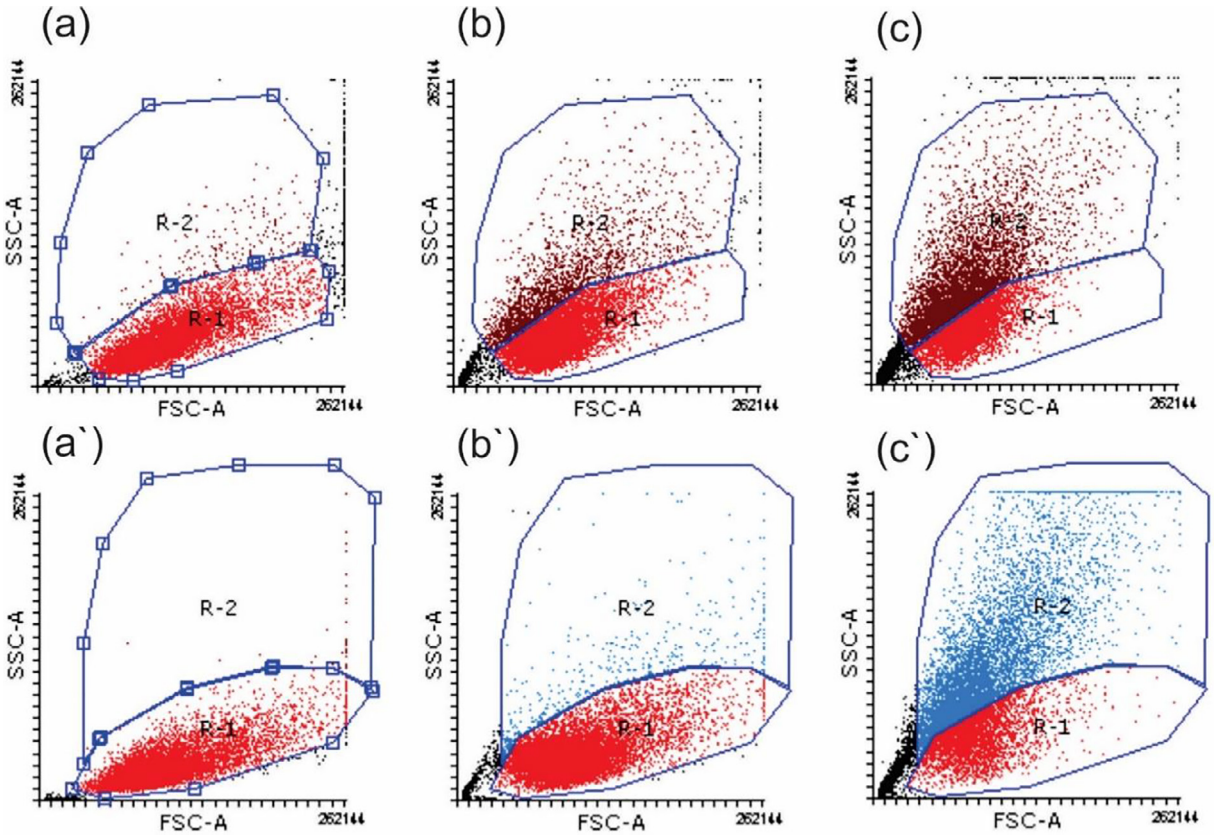

Fig. 10. Flow cytometry cytogram of SSC and FSC: (a, b, c) showing PC3 cells with a concentration of 0, 100, and 500 μg/ml of magnetite nanoparticles respectively and (a', b', c') presenting BPH1 SSC cytogram with the same concentration.

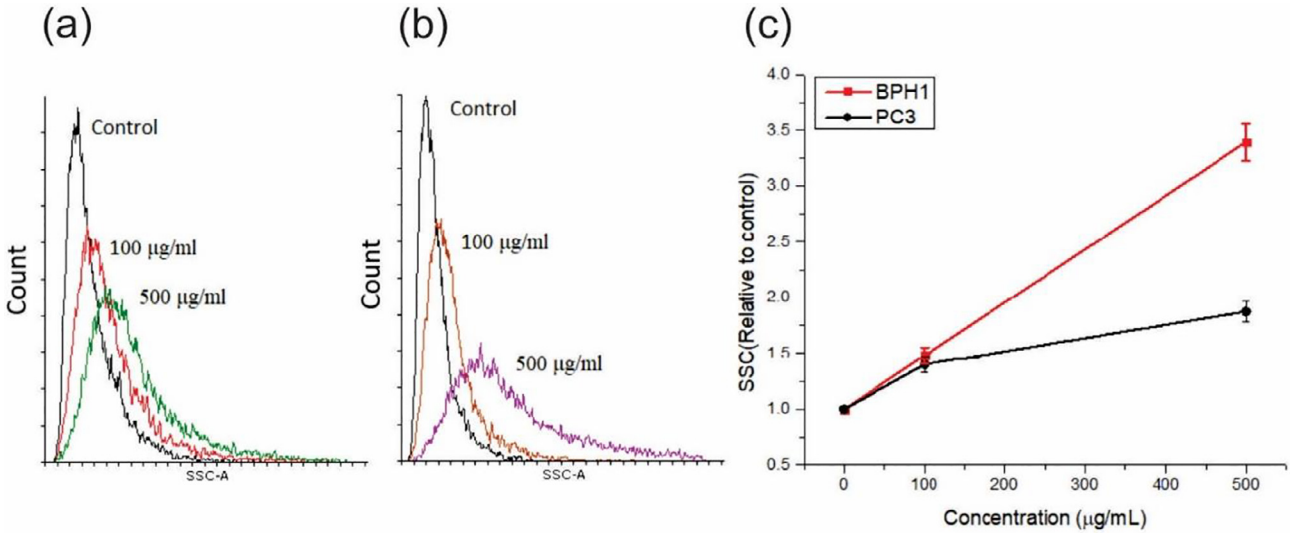

Fig. 11. (a, b) Flow cytometric analysis of PC3 and BPH1, resp. SSC increases with increasing concentration in both cells by MNP treatment. (c) SSC (relative to control) changes with concentration for PC3 (black line) and BPH1 (red line). (For interpretation of the references to colour in this figure legend, the reader is referred to the web version of this article.)

exposure of nanoparticles to the cells, first of all the nanoparticles adhere to the surface and subsequently, due to endocytosis, they internalize to the cells followed by agglomeration inside the cells (s. Figs. 6–9) [23]. In the case of PC3 cells (s. Fig. 8), it is obvious that with increasing concentration of coated particles, the cells take up more particles which accumulate in bigger agglomerations. In contrast, the benign cells take up particles at the lower levels in comparison with PC3 prostate cancer cells. The same results were obtained for the both conditions, 100 and 500 μg/ml of particles (s. Fig. 9), which is in agreement with previous studies [17]. Collectively, our data indicated that the prostate cancer cells take up the coated particles with higher efficiency than benign cells. In contrast to the treatment by coated particles, treatment with MNP shows different result which indicated the effect of surface structure in cellular uptake of NP [27]. In contrast to the coated MNP, treatment of cells with the uncoated NPs, results in more particles internalized to the normal cells-BPH1 (related to the

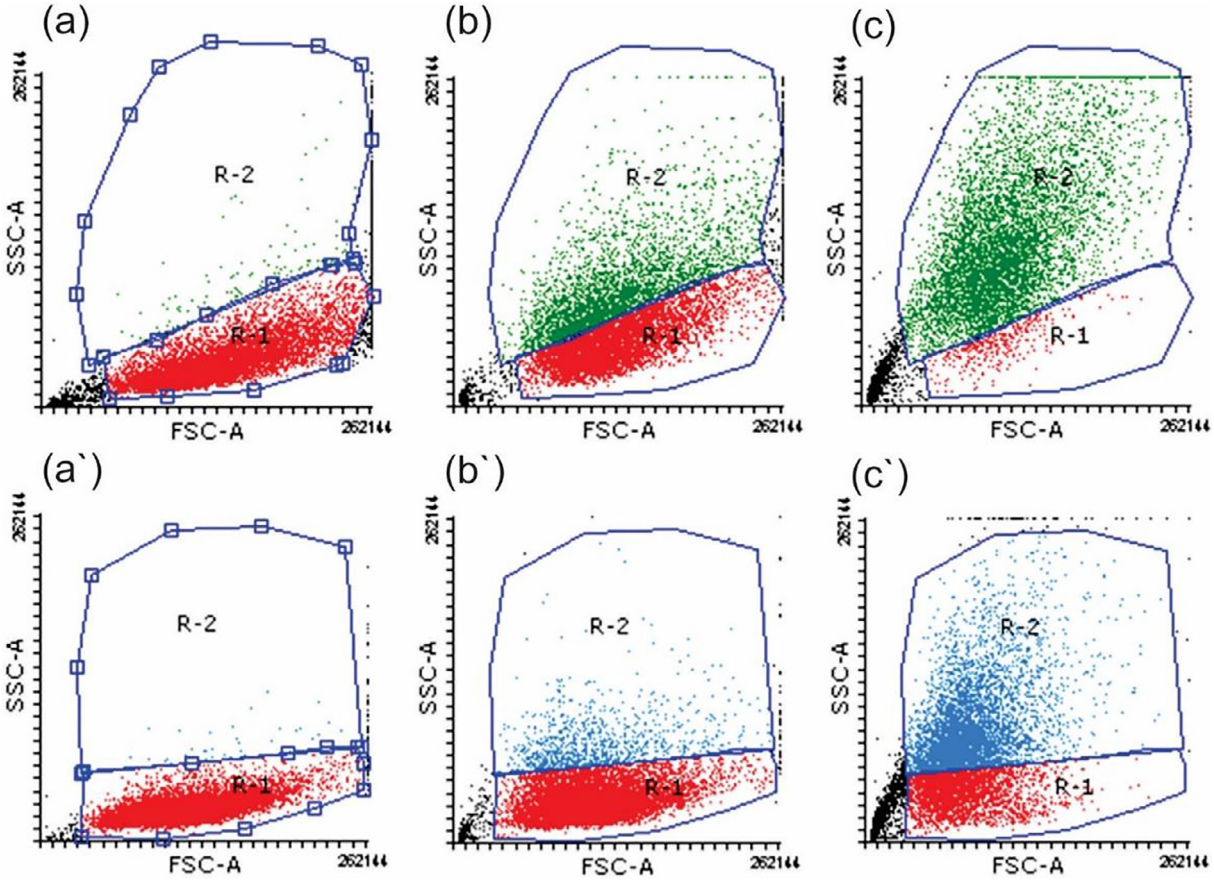

Fig. 12. Flow cytometry cytogram of SSC and FSC: (a, b, c) showing PC3 cells with a concentration of 0, 100, and 500 μg/ml of aminosilane coated respectively and (a', b', c') presenting BPH1 SSC cytogram with the same concentration.

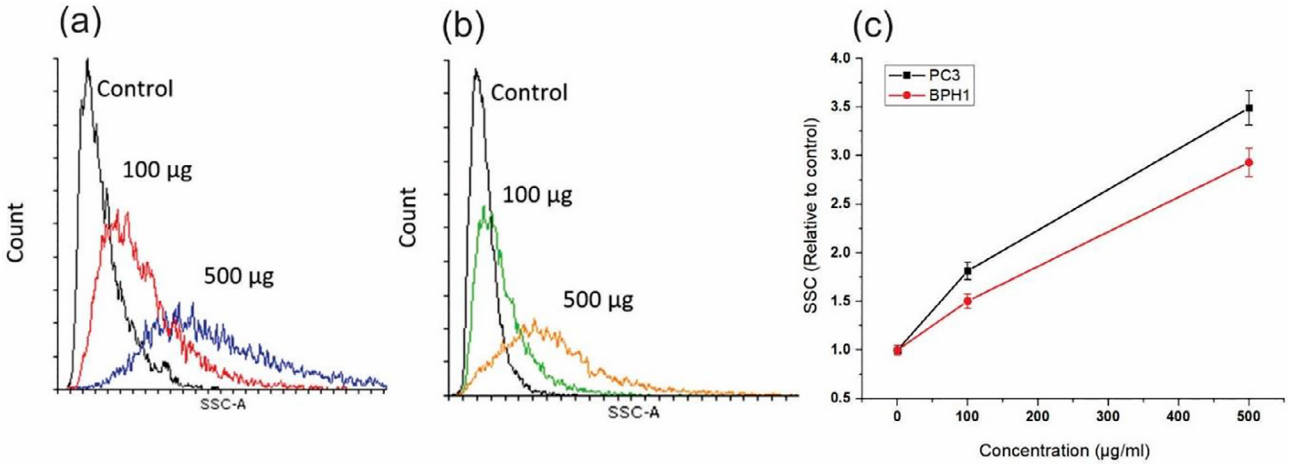

Fig. 13. (a, b) Flow cytometric analysis of PC3 and BPH1, resp. SSC increases with increasing concentration in both cells. (c) SSC (relative to control) changes with concentration for PC3 (black line) and BPH1 (red line). (For interpretation of the references to colour in this figure legend, the reader is referred to the web version of this article.)

negative control) in comparison to cancer cells (s. Figs. 6 and 7). There are different factors that may affect the nanoparticles uptake efficiency such as charge, size, shape and surface modification of the nanoparticles itself as well as cell types [28]. The interaction of cells is also different with the negatively and positively charged particles because of electrostatic properties [29]. The efficiency of the cellular NP uptake could be different among the various cells and this is mainly due to the cell type specific features of various cells and cell dynamics. Several endocytic pathways can regulate the nanoparticles entry to the cells, such as pinocytosis, clathrin or caveolin dependent and clatherin-caveolon independent pathways [30]. In the same line of evidence, Chaves and colleagues showed that the breast cancer cells uptake with higher efficiency NP than normal cells [31]. They reported this is via a clathrin-dependent endocytosis pathway and cancerous cell line express higher amount of clathrin but not caveolin than normal cells. However, the exact mechanism that cells decide, from which pathway uptake the NP need further investigations.

To quantify the uptake of nanoparticles by the cells in a dose

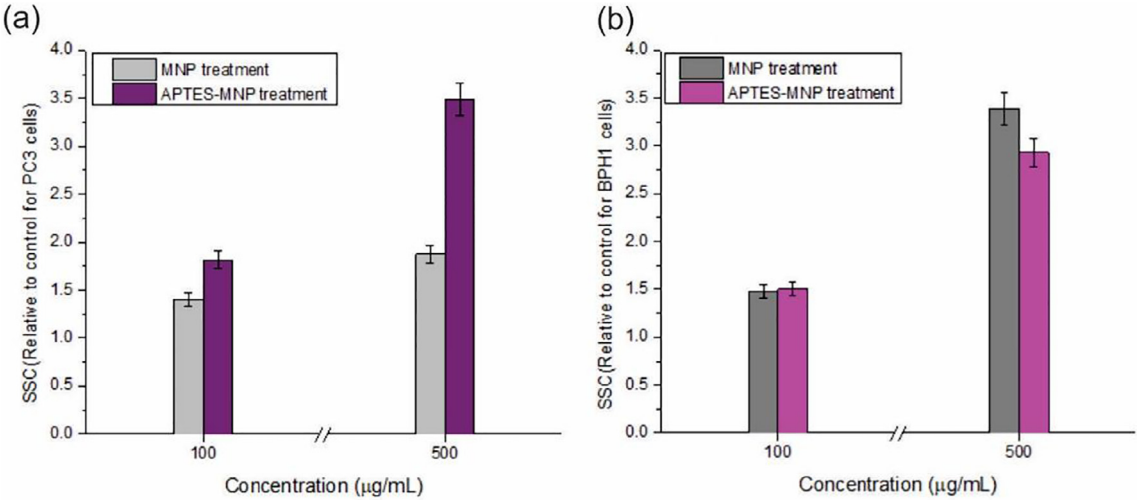

Fig. 14. SSC (relative to control) changes with 100 and 500 μg/mL of MNP and APTES-MNP for PC3 cells (a) and BPH1 (b).

dependent comparison, flow cytometry measurements have been applied. This allows determining the magnetite nanoparticles internalization by PC3 and BPH1 cells. The flow cytometry results of treatment with MNP to the cells are presented in Figs. 10 and 11 and with APTES-MNP are illustrated in Figs. 12 and 13. Flow cytometry measurements evaluated reactions of cells to magnetite nanoparticles with 0 (as a control), 100 and 500 μg/ml concentration quantitatively after treatment and incubation for 24 h [32,33]. Forward scatter (FSC) and side scatter (SSC) are two parameters to assess and observe the cellular uptake. Forward light scattering gives information about the cell size and side scattering about the internal structure, organelles and generally internal complexity [34–37]. As shown in Fig. 10 and Fig. 12, SSC signals grow with increasing concentration of the particles which demonstrates higher uptake of particles. In contrast, FSC intensity decreases with increasing APTES-MNP concentration that is explained because of absorbing and reflecting the light from nanoparticles [33]. To distinguish between cells with particles and without particles, two regions were defined. R-1 was used to clarify the control cell samples and R-2 was used to show cells after treatment with different concentration. These tests revealed that the cells with 500 μg/ml of particles treatment exhibit a huge growth in size. As expected, these experiments also demonstrate the same trend for BPH1.

Fig. 10 presents the application result of MNP to both cell lines. In flow cytometry histogram granularity of the cells does not show significant changes between PC3 and BPH1 but in flow cytometric analysis (Fig. 11) which concern to untreated control, granularity of BPH1 cells increased more than cancer cells.

The evaluation of dose dependent uptake of APTES-MNP is plotted in Fig. 13 (a, b for PC3 and BPH1 cells, resp.). It is obvious that the SSC intensity increases with increasing concentration for PC3 and similarly for BPH1. Mean side scatter changes are also plotted in Fig. 13c.

Consistently, the TEM and flow cytometry results indicate that PC3 (cancerous) uptakes with higher rates coated particles and BPH1 uncoated particles. The overall analysis of flow cytometry measurement is shown in Fig. 14.

4. Conclusion

In summary, we investigated *in vitro* cellular uptake of magnetite and aminosilane coated magnetite nanoparticles by cancer prostate cells (PC3) and prostate benign cells (BPH1). The nanoparticles were synthesized by a wet chemical method (co-precipitation method) using hydrolysis of two iron salts, ferric chloride and ferrous sulfate, and co-precipitation by ammonium hydroxide and at the end were coated with APTES which increases biocompatibility and stability of nanoparticles. Intracellular uptake of particles to cells was investigated by transmission electron microscopy and flow cytometry. It was demonstrated that cellular uptake of particles is cell type dependent. It was also shown that prostate cancer cells take up the coated nanoparticles with a significantly higher level than benign cells which are considered as normal cells. In addition, our experiments indicate the higher uptake of uncoated particles by BPH1 cells that can be due to the cell type specific mechanism of the NP uptake. According to TEM figures, we did not observe the interaction among the NP and cell organelles.

Acknowledgment

MY acknowledges financial support of the Düsseldorf School of Oncology, Heinrich-Heine University Düsseldorf, FH of the European Network on Noonan Syndrome and Related Disorders (NSEuroNet), and SNR of the German Federal Ministry of Education and Research (BMBF) – German Network of RASopathy Research (GeNeRARe). We are also grateful to Center for Advance Imaging (CAi) and Institute of Anatomy I, especially Elisabeth Wesbuer, Heinrich-Heine University Düsseldorf, for the TEM experiments.

References

[1] A. Ito, M. Shinkai, H. Honda, T. Kobayashi, Medical application of functionalized magnetic nanoparticles, J. Biosci. Bioeng. 100 (2005) 1–11.
[2] T.K. Jain, M.A. Morales, S.K. Sahoo, D.L. Leslie-Pelecky, V. Labhasetwar, Iron oxide nanoparticles for sustained delivery of anticancer agents, Mol. Pharm. 2 (2005) 194–205.
[3] S.B.D. Makhluf, R. Abu-Mukh, S. Rubinstein, H. Breitbart, A. Gedanken, Modified PVA–Fe_3O_4 nanoparticles as protein carriers into sperm cells, Small 4 (2008) 1453–1458.
[4] Q.A. Pankhurst, J. Connolly, S. Jones, J. Dobson, Applications of magnetic nanoparticles in biomedicine, J. Phys. D Appl. Phys. 36 (2003) R167.
[5] M. Babic, D. Horák, M. Trchová, P. Jendelová, K. Glogarová, P. Lesný, V. Herynek, M. Hájek, E. Syková, Poly (L-lysine)-modified iron oxide nanoparticles for stem cell labeling, Bioconjug. Chem. 19 (2008) 740–750.
[6] J.W. Bulte, T. Douglas, B. Witwer, S.-C. Zhang, E. Strable, B.K. Lewis, H. Zywicke, B. Miller, P. van Gelderen, B.M. Moskowitz, Magnetodendrimers allow endosomal magnetic labeling and in vivo tracking of stem cells, Nat. Biotechnol. 19 (2001) 1141.
[7] A. Carmona-Ribeiro, F. Ortis, R. Schumacher, M. Armelin, Interactions between cationic vesicles and cultured mammalian cells, Langmuir 13 (1997) 2215–2218.
[8] P.A. Dresco, V.S. Zaitsev, R.J. Gambino, B. Chu, Preparation and properties of magnetite and polymer magnetite nanoparticles, Langmuir 15 (1999) 1945–1951.
[9] H.S. Lee, E.H. Kim, H. Shao, B.K. Kwak, Synthesis of SPIO-chitosan microspheres for MRI-detectable embolotherapy, J. Magn. Magn. Mater. 293 (2005) 102–105.
[10] M. Lewin, N. Carlesso, C.-H. Tung, X.-W. Tang, D. Cory, D.T. Scadden, R. Weissleder, Tat peptide-derivatized magnetic nanoparticles allow in vivo tracking and recovery of progenitor cells, Nat. Biotechnol. 18 (2000) 410.
[11] Y. Zhang, J. Zhang, Surface modification of monodisperse magnetite nanoparticles for improved intracellular uptake to breast cancer cells, J. Colloid Interface Sci. 283 (2005) 352–357.

[12] E. Asenath Smith, W. Chen, How to prevent the loss of surface functionality derived from aminosilanes, Langmuir 24 (2008) 12405–12409.
[13] S. Giri, B.G. Trewyn, M.P. Stellmaker, V.S.Y. Lin, Stimuli-responsive controlled-release delivery system based on mesoporous silica nanorods capped with magnetic nanoparticles, Angew. Chem. Int. Ed. 44 (2005) 5038–5044.
[14] Y. He, S. Wang, C. Li, Y. Miao, Z. Wu, B. Zou, Synthesis and characterization of functionalized silica-coated Fe3O4 superparamagnetic nanocrystals for biological applications, J. Phys. D Appl. Phys. 38 (2005) 1342.
[15] K. Herve, L. Douziech-Eyrolles, E. Munnier, S. Cohen-Jonathan, M. Souce, H. Marchais, P. Limelette, F. Warmont, M. Saboungi, P. Dubois, The development of stable aqueous suspensions of PEGylated SPIONs for biomedical applications, Nanotechnology 19 (2008) 465608.
[16] K.K. Selim, Y.-S. Ha, S.-J. Kim, Y. Chang, T.-J. Kim, G.H. Lee, I.-K. Kang, Surface modification of magnetite nanoparticles using lactobionic acid and their interaction with hepatocytes, Biomaterials 28 (2007) 710–716.
[17] A. Jordan, R. Scholz, P. Wust, H. Schirra, T. Schiestel, H. Schmidt, R. Felix, Endocytosis of dextran and silan-coated magnetite nanoparticles and the effect of intracellular hyperthermia on human mammary carcinoma cells in vitro, J. Magn. Magn. Mater. 194 (1999) 185–196.
[18] A. Jordan, P. Wust, R. Scholz, B. Tesche, H. Fähling, T. Mitrovics, T. Vogl, J. Cervos-Navarro, R. Felix, Cellular uptake of magnetic fluid particles and their effects on human adenocarcinoma cells exposed to AC magnetic fields in vitro, Int. J. Hyperth. 12 (1996) 705–722.
[19] R.S. Molday, in, Google Patents, 1984.
[20] M. Ma, Y. Zhang, W. Yu, H.-Y. Shen, H.-Q. Zhang, N. Gu, Preparation and characterization of magnetite nanoparticles coated by amino silane, Colloids Surf., A 212 (2003) 219–226.
[21] T. Mosmann, Rapid colorimetric assay for cellular growth and survival: application to proliferation and cytotoxicity assay, J. Immunol. Methods 65 (1983) 55–63.
[22] A.M. Atta, H.A. Al-Lohedan, S.A. Al-Hussain, Functionalization of magnetite nanoparticles as oil spill collector, Int. J. Mol. Sci. 16 (2015) 6911–6931.
[23] A. Tomitaka, A. Hirukawa, T. Yamada, S. Morishita, Y. Takemura, Biocompatibility of various ferrite nanoparticles evaluated by in vitro cytotoxicity assays using HeLa cells, J. Magn. Magn. Mater. 321 (2009) 1482–1484.
[24] R. Waldron, Infrared spectra of ferrites, Phys. Rev. 99 (1955) 1727.
[25] R. Cornell, U. Schwertmann, Structure, Properties, Reactions, Occurrence and Uses, The Iron Oxides, VCH, Weinheim, 1996, pp. 375–395.
[26] S. Naqvi, S. Mohammad, M.Z. Abdin, F.J. Ahmed, A.N. Maitra, C.K. Prashant, A.K. Dinda, Concentration-dependent toxicity of iron oxide nanoparticles mediated by increased oxidative stress, Int. J. Nanomed. 5 (2010) 983.
[27] A. Jordan, R. Scholz, Klaus Maier-Hauff, Manfred Johannsen, Peter Wust, Jacek Nadobny, Hermann Schirra, et al., Presentation of a new magnetic field therapy system for the treatment of human solid tumors with magnetic fluid hyperthermia, J. Magn. Magn. Mater. 225 (2001) 118–126.
[28] Jia Hu, Yaling Liu, Cyclic strain enhances cellular uptake of nanoparticles, J. Nanomater. 16 (1) (2015) 291.
[29] Sara Salatin, Solmaz Maleki Dizaj, Ahmad Yari Khosroushahi, Effect of the surface modification, size, and shape on cellular uptake of nanoparticles, Cell Biol. Int. 39 (8) (2015) 881–890.
[30] G. Sahay, D.Y. Alakhova, A.V. Kabanov, Endocytosis of nanomedicines, J. Control Release 145 (2010) 182–195.
[31] N.L. Chaves, E.-L. Irina, J. Böttner, C.A.P. Lopes, B.C. Guido, A.R. de Sousa, S.N. Báo, Exploring cellular uptake of iron oxide nanoparticles associated with rhodium citrate in breast cancer cells, Int. J. Nanomed. 12 (2017) 5511.
[32] M. Brown, C. Wittwer, Flow cytometry: principles and clinical applications in hematology, Clin. Chem. 46 (2000) 1221–1229.
[33] R. Zucker, E. Massaro, K. Sanders, L. Degn, W. Boyes, Flow cytometry concepts and capabilities to assess environmental contaminants, Cytometry 77 (2010) 677–685.
[34] J.S. Aaron, N. Nitin, K. Travis, S. Kumar, T.G. Collier, S.Y. Park, M.J. Yacaman, L. Coghlan, M. Follen, R.R. Richards-Kortum, Plasmon resonance coupling of metal nanoparticles for molecular imaging of carcinogenesis in vivo, J. Biomed. Opt. 12 (2007) 034007.
[35] H.M. Shapiro, Optical measurements in cytometry: light scattering, extinction, absorption, and fluorescence, Methods Cell Biol. 63 (2001) 107–129.
[36] H.B. Steen, Flow cytometer for measurement of the light scattering of viral and other submicroscopic particles, Cytometry Part A 57 (2004) 94–99.
[37] R.M. Zucker, K.H. Elstein, R.E. Easterling, E.J. Massaro, Flow cytometric discrimination of mitotic nuclei by right-angle light scatter, Cytometry Part A 9 (1988) 226–231.